Chemical Engineering Journal 308 (2017) 289–298

Contents lists available at ScienceDirect

Chemical Engineering Journal

journal homepage: www.elsevier.com/locate/cej

Effects of the size and Cu modulation of Pd_n ($n \leqslant 38$) clusters on Hg^0 adsorption

Lixia Ling [a], Lili Fan [a], Xue Feng [a], Baojun Wang [b,*], Riguang Zhang [b]

[a] College of Chemistry and Chemical Engineering, Taiyuan University of Technology, Taiyuan 030024, Shanxi, PR China
[b] Key Laboratory of Coal Science and Technology (Taiyuan University of Technology), Ministry of Education and Shanxi Province, Taiyuan 030024, Shanxi, PR China

HIGHLIGHTS

- AC can enhance the stability of magic clusters Pd_n (n = 4, 6, 8, 13, 19, 23).
- Pd_n cluster size influences Hg^0 adsorption greatly, and Pd_{13}/AC is optimal.
- $CuPd_{12}$, Cu_2Pd_{11} and Cu_6Pd_7 bimetallic clusters are relatively easy to obtain.
- The adsorption of Hg^0 is affected by Cu doping ratio, and Cu_2Pd_{11}/AC is the best.

GRAPHICAL ABSTRACT

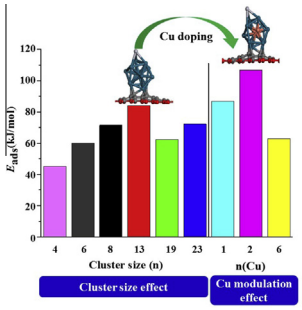

ARTICLE INFO

Article history:
Received 25 July 2016
Received in revised form 30 August 2016
Accepted 1 September 2016
Available online 8 September 2016

Keywords:
Size effect
Cu modulation
Hg^0 adsorption
Activated carbon supported Pd_n ($n \leqslant 38$) clusters

ABSTRACT

A density functional theory (DFT) method was used to study the adsorption of Hg^0 on activated carbon supported Pd_n ($n \leqslant 38$) clusters, the size and Cu modulation of Pd clusters were investigated. The adsorption energies of Hg^0 on Pd_n/AC (n = 4, 6, 8, 13, 19, 23) show that the strongest adsorption strength is on the Pd_{13}/AC. AC can prevent Pd clustering to a bulk and disperse cluster on the surface by comparing the interaction energy of Pd_n cluster on AC with the binding energy per atom of corresponding Pd_n cluster. Furthermore, some of Pd atoms in Pd_{13} cluster were substituted by Cu atoms to improve the adsorption of Hg^0 and reduce the dosage of Pd. $CuPd_{12}$, Cu_2Pd_{11} and Cu_6Pd_7 are the most stable bimetallic clusters. In addition, the adsorption of Hg^0 shows that Cu_2Pd_{11}/AC is the most effective adsorbent for Hg^0.

1. Introduction

The removal of Hg^0 has caused wide public concerns and been studied by many researchers due to its low water solubility and chemical reactivity [1,2]. Different materials are adopted as sorbents for removing Hg^0, including non-noble metal Cu [3], and metal oxides ZnO [4,5], CuO [6], V_2O_5 [7] and Fe_2O_3 [8]. However, the capture ability of Hg^0 is weak due to little adsorption energies of Hg^0 on surfaces of these materials [4,5,9–11]. Therefore, Hg^0 is needed to be oxidized to oxides, followed by the removal of the oxidized mercury on account of a strong interaction between sorbents and oxidized mercury [12]. The above technical process is complex. It is known that noble metals, especially Pd, have high direct Hg^0 capture efficiency [13,14].

The adsorptions of Hg^0 on 22 pure metals were studied, and it was found that Pd is the most promising sorbent with the strongest Hg^0 adsorption capacity [15]. Also, the adsorption strength of Hg^0 on Ag, Au, Pt and Pd surfaces was an increased order, and the adsorption energies of Hg^0 on perfect and defected Pd(1 1 1) surface are 81.0 and 217.1 $kJ \cdot mol^{-1}$, respectively [16], higher than that

* Corresponding author at: No. 79 West Yingze Street, Taiyuan 030024, PR China.
E-mail addresses: linglixia@tyut.edu.cn (L. Ling), wangbaojun@tyut.edu.cn (B. Wang).

http://dx.doi.org/10.1016/j.cej.2016.09.004
1385-8947/

on perfect and defected Au(1 1 1) surface with adsorption energies of 40.5 and 53.1 kJ·mol^{-1}, respectively [17]. Nevertheless, the high price of Pd limits its wide application [18].

When the bulk size of noble metals was reduced to metal clusters containing only a few atoms, the loading amount of the noble metals can be largely reduced, as well as show unique chemical and physical properties [19,20]. Pd_n clusters have been widely used in the treatment of automobile exhaust gas [21,22] for the high activity in heterogeneous catalytic reactions [23]. The catalytic activity of Pd_n clusters is influenced greatly by the quantum size effect, and which can be improved by adjusting the size dimension, shown in the adsorptions of CO and NO, as well as the CO + NO reaction on Pd_n clusters [23,24]. Similarly, adjusting the amount of loaded Pd on γ-Al_2O_3 can enhance the removal efficiency of Hg^0 [16]. Therefore, obtaining the optimal size of Pd_n cluster is very meaningful.

Graphene-based materials are as superior adsorbents for removing aromatic compounds from effluent [25], uranium from groundwater [26], and so on. In addition, the injection of graphite with 10% Pd resulted in a decrease of 98.2% of the total Hg concentration in a gas mixture consisting of ~11,000 ng/Nm^3 Hg, while injection of the single-walled carbon nanotubes (SWNT) with 10% Pd resulted in a decrease of 95.4% of the total Hg [27]. AC is one of graphene-based materials with large surface area and unique structure. The combination of AC and Pd may be an effective Hg^0 remover [28], in view of the high Hg^0 removal efficiency of Pd and specific surface of AC [29]. The removal efficiency of Hg^0 increased with the increasing of Pd loading amount on AC, but the effective utilization rate of loaded Pd decreased significantly simultaneously [14]. The removal efficiencies of Hg^0 are various with different supports. Thus, the effect of AC on the removal of Hg^0 is needed to be explored.

Additionally, the second metal doping can improve the catalytic activity of pure metals [30]. The alloying treatment of Pd_n clusters increased the energy conversion rate of fuel cell [31,32]. Among all metals, Cu is one of non-noble metals, which is usually doped into the noble metal to reduce the cost of materials, as well as promote the stability and reactivity [33,34]. The addition of Cu into Pd/Al_2O_3 and Pd/SiO_2 can enhance the stability of the catalyst [33]. Moreover, MPd_{12} (M = Fe, Co, Ni, Cu, Zn) supported on the graphene with single vacancy (SV-G) show higher catalytic activity to the oxygen reduction reaction than that of Pd_{13}/SV-G, in which $CuPd_{12}$ has the strongest interaction with the SV-G surface [34]. However, the effect of Cu modulation of Pd_n/AC on the adsorption of Hg^0 is unclear.

In this work, the size effect of Pd_n ($n \leqslant 38$) clusters on Hg^0 adsorption will be studied. The magic clusters of Pd_n ($n \leqslant 38$) are obtained and are loaded on the AC. Then, the optimal size of loaded Pd_n cluster is obtained by investigating adsorptions of Hg^0 on different Pd_n clusters supported on the AC. Meanwhile, the effect of AC will be analyzed. Additionally, the optimal Pd_n cluster will be modulated by Cu with different ratios to improve Hg^0 adsorption and reduce the dosage of Pd. The configurations and stability of different Cu-Pd bimetallic clusters are studied, and then, the adsorptions of Hg^0 on stable AC supported Cu-Pd bimetallic clusters are discussed to obtain the optimized Cu doping ratio.

2. Calculation method and model

2.1. Computation method

All calculations were performed by the DMol^3 program package [35] in Materials Studio 5.5. The exchange and correlation energies were calculated using generalized gradient approximation (GGA) with Perdew-Wang exchange-correlation functional (PW91) [36,37]. There are two main reasons for choosing the GGA-PW91 in the present work. Firstly, the binding energies of Pd atom on the single vacancy AC surface were calculated at PW91, Perdew-Burke-Ernzerhof (PBE) and Becke' hybrid exchange functional and the Lee-Yang-Parr (BLYP) functionals, which are 516.5, 506.7 and 441.2 kJ·mol^{-1}. The similar results are obtained by PW91 and PBE functionals, which agree with the theoretical result of 518.1 kJ·mol^{-1} by Ma et al. [38]. Secondly, PW91 function satisfies the known formal properties of the exact exchange-correlation functional [39], and which is widely used to study the structure and properties of Pd clusters [40–42]. Equivalent to 6-31G** in Gaussian [43,44], the double numerical plus polarization (DNP) basis set [45] was employed for the valence electron functions. An all-electron basis set was applied to deal with carbon atoms, while relativistic effects were considered for Cu, Pd and Hg atoms with the inner electrons kept frozen and replaced by an effective core potentials (ECP) [46]. The Brillouin zone integrations within the Monkhorst Pack were $3 \times 3 \times 1$ *k*-point according to the test and reported results [47,48]. A cutoff of 4.6 Å is chosen and a smearing of 0.005 Ha (1 Ha = 2625.5 kJ·mol^{-1}) to the orbital occupation is applied to achieve accurate electronic convergence. For geometrical optimizations, the total energy, the maximum force and the maximum displacement were converged to 2×10^{-5} Ha, 4×10^{-3} Ha/Å and 0.005 Å, respectively. Spin polarization was performed considering that the carbon vacancies can induce magnetism by breaking the symmetry of the nonmagnetic perfect surface [49].

2.2. Surface model

As shown in our previous study [50], a single-layer $p(6 \times 6)$ graphite was taken to simulate AC surface by cleaving the optimized graphite structure with 71 carbon atoms, and a single carbon atom vacancy was on the surface [51,52]. The edge was fixed to minimize elastic interactions between periodic vacancy defects [51,53], as red spheres shown in Fig. 1. The Pd_n clusters were constructed by adding one Pd atom to various possible binding sites of the preceding stable cluster. The structure was regarded as the most stable configuration with the lowest total energy and highest average binding energy in the isomers. As for the construction of Cu-Pd bimetallic clusters, one Pd atom in Pd_{13} was substituted by Cu leading to $CuPd_{12}$, and then another one was substituted from the preceding stable Cu-Pd bimetallic cluster leading to Cu_m-Pd_{n-m} (m = 2–6). The similar method was applied to obtain Cu_m-Pd_{n-m} (m = 12–7), in which one Cu atom in Cu_{13} was substituted by a Pd forming $Cu_{12}Pd$. Based on the reports [54,55], the site with the smallest substitution energy is preferred for the Cu substitution, and a bigger average binding energy corresponds to a higher stability. The average binding energy $E_b(Pd_n)$, $E_b(Cu_mPd_{n-m})$ and substitution energy E_{sub} are defined as follows:

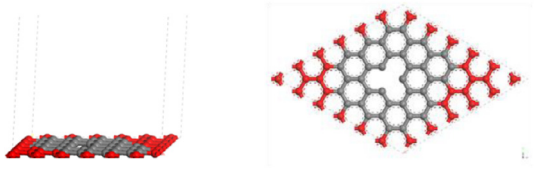

AC(a) AC(b)

Fig. 1. The optimized slab model of the AC surface. (a) and (b) are the side view and top view of the AC surface, respectively. (The red and dark grey spheres represent the fixed and relaxation carbon atoms, respectively.). (For interpretation of the references to colour in this figure legend, the reader is referred to the web version of this article.)

$$E_b(Pd_n) = [nE(Pd) - E(Pd_n)]/n \quad (1)$$

$$E_b(Cu_mPd_{n-m}) = [mE(Cu) + (n-m)E(Pd) - E(Cu_mPd_{n-m})]/n \quad (2)$$

$$E_{sub} = [E(Cu_mPd_{n-m}) + mE(Pd) - E(Pd_n) - mE(Cu)]/m \quad (3)$$

where E(Pd) and E(Cu) represent total electronic energies of Pd atom and Cu atom, respectively; $E(Pd_n)$ and $E(Cu_mPd_{n-m})$ are total electronic energies of Pd_n clusters and Cu-Pd bimetallic clusters, respectively; n and m are numbers of Pd atoms and substituted Cu atoms; $E_b(Pd_n)$ and $E_b(Cu_mPd_{n-m})$ are used to estimate the stability of Pd_n clusters and Cu-Pd bimetallic cluster; and E_{sub} reflects the substitution ability of Cu atom. A bigger value of E_b means a more stable Pd_n cluster and Cu-Pd bimetallic cluster, while a more negative value of E_{sub} implies an easier substitution of Cu atom [54,55].

3. Results and discussion

3.1. Hg^0 adsorption on the Pd/AC surface

Firstly, the structure of AC loading a Pd atom (Pd/AC) and the adsorption of Hg^0 on the Pd/AC surface are discussed. The result shows that the isolated Pd atom has a strong affinity to the C-defected site on the AC surface with an adsorption energy of 516.5 kJ·mol^{-1}. In addition, there's a weak interaction between Hg^0 and the Pd/AC surface, with a little adsorption energy of 30.1 kJ·mol^{-1}, implying that Pd/AC is not an efficient mercury sorbent. Differently, Pd has been demonstrated that it has a high Hg^0 removal efficiency in theory and experiment [14,56]. Steckel et al. [3] found that the order of the interaction strength between Hg^0 and different metal surfaces is Ag < Au < Cu < Ni < Pt < Pd. And the adsorption energy of Hg^0 on the defected Pd(1 1 1) surface is 217.1 kJ·mol^{-1}, higher than that on the perfect surface with 81.0 kJ·mol^{-1} [16]. The high Hg^0 removal efficiency of metallic Pd has also been verified by the packed-bed reactor system, and the amount of Hg^0 in simulated fuel gases was measured via the online atomic fluorescence spectrophotometer [57]. In addition, some clusters show stronger adsorption capacity than the surface. The adsorption energy of H_2 on the Pd cluster is larger than that on the Pd surface [58], and similar cases for adsorptions of CO, H, O_2 and O on the Pt_{55} cluster and Pt(1 1 1) surface [59]. It can be seen that proper clustering with a certain amount of atoms can improve the activity of metal greatly, and the aggregative state of Pd atoms will be studied to capture Hg^0.

3.2. The evolution of Pd_n (n = 2–8, 13, 19, 23, 38) clusters and their stabilities

The stable configurations of Pd_n (n = 2–8) clusters are obtained by calculations, which are made comparison with the literature report [41,42,60]. Therefore, the reliability of the calculation method and parameters adopted in the study will be verified. For the Pd clusters with the more Pd atoms (13, 19, 23 and 38), the stable configurations are obtained based on the results in literature [61–65].

3.2.1. The evolution of Pd_n (n = 2–8) clusters

The possible structures and corresponding total energies for Pd_n (n = 2–8) clusters are shown in Fig. S1 and Table S1 in the Supporting Information. In Fig. 2, we just show the most stable configurations of Pd_n (n = 2–8) clusters. For Pd_2 dimer, the linear structure is the only existent form with a bond length of 2.560 Å, close to the reported values of 2.565 and 2.555 Å [40,41]. When adding one Pd atom to the linear Pd_2 cluster, we can obtain a triangular Pd_3 cluster, with the average bond length of 2.578 Å, in agreement with the reported value of 2.589 Å [40]. Also, the bond angle (60°) is consistent with the result by Nava et al. [66]. The stable Pd_4 cluster is tetrahedral, and the average bond length is 2.661 Å, which is the same as the reported value [40]. For Pd_5 cluster, the most stable configuration is trigonal bipyramid, with the average bond length of 2.677 Å between the apex and equatorial atom, close to the reported value of 2.660 Å [67]. Among the three isomers of Pd_6 cluster, the octahedron Pd_6 is the most stable configuration with the lowest energy, and the bond length between the apex and equatorial atom is 2.702 Å, close to the reported value of 2.690 Å [67]. There are two isomers for Pd_7 cluster, and the pentagonal bipyramid Pd_7 cluster is relatively more stable, with a bond length of 2.727 Å from the apex to equatorial atom, also close to the reported value of 2.760 Å [67]. For Pd_8 cluster, three isomers are obtained, and the bicapped octahedral Pd_8 cluster is the most stable configuration, the average bond length is 2.706 Å, in agreement with the literature value of 2.747 Å [68]. It can be seen that for a given Pd_n cluster, the isomer with a higher symmetry is more stable, in line with the literature reports [69].

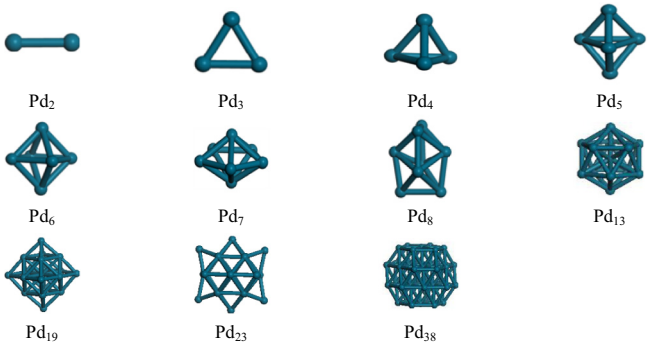

Fig. 2. The most stable configurations of Pd_n (n = 2–8, 13, 19, 23, 38) clusters.

3.2.2. The stability of Pd_n (n = 2–8, 13, 19, 23, 38) clusters

The average binding energies (E_b) per atom of Pd_n (n = 2–8) clusters are calculated to investigate the stability. The relationship between E_b and the cluster size is shown in Fig. 3(a), in which the black line represents the variation trends of calculated values, while the red line is that of the literature values [41,60]. It can be seen that with the increase of Pd_n cluster size, the average binding energy increases monotonously, implying an enhancement of the stability of Pd_n (n = 2–8) clusters. Besides, our calculated results give the same stability ranking for the Pd cluster as in the previous work [41], which confirms the rationality of the computation method and parameters further.

Magic clusters are species with particular stability, and are measured by mass spectroscopy in experiment [70]. To obtain the stable magic clusters with different sizes by theoretical method, the second energy difference Δ_2E is calculated [61,63,71], which is defined as follows:

$$\Delta_2E = E(Pd_{n+1}) - 2E(Pd_n) + E(Pd_{n-1}) \quad (4)$$

$$\Delta E_0 = E(Pd_{n+1}) - E(Pd) - E(Pd_n) \quad (5)$$

$$\Delta E_1 = E(Pd_n) - E(Pd) - E(Pd_{n-1}) \quad (6)$$

where $E(Pd_n)$, $E(Pd_{n+1})$ and $E(Pd_{n-1})$ represent energies of Pd_n cluster, Pd_{n+1} cluster and Pd_{n-1} cluster, respectively. Δ_2E is the energy difference between ΔE_0 and ΔE_1 for fragmentation paths of $Pd_{n+1} \rightarrow Pd_n + Pd$ and $Pd_n \rightarrow Pd_{n-1} + Pd$, and a positive value means an easier dissociation of Pd_{n+1} cluster than that of Pd_n cluster. The magic clusters are identified by comparing the Δ_2E, which is more stable than its lighter and heavier neighbors and considered as a measure of the stability of the clusters [72].

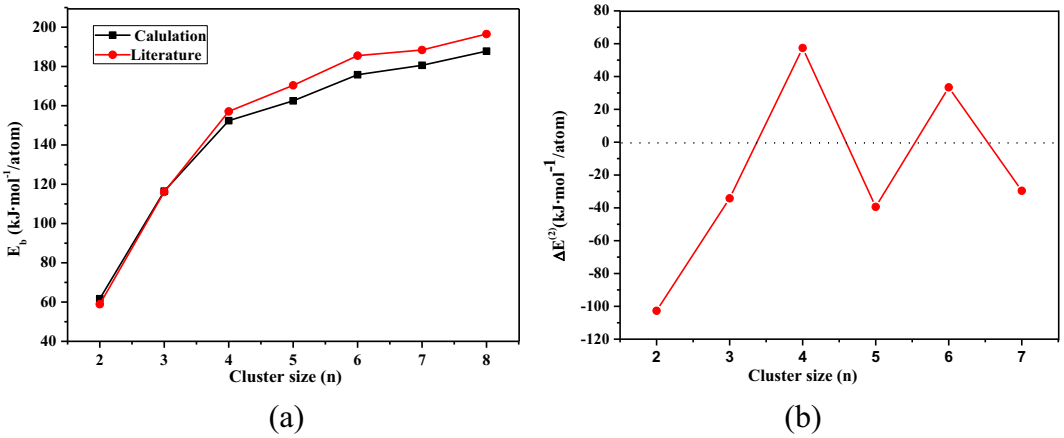

Fig. 3. (a) The variation trend of the average binding energies with the cluster size; (b) the variation trend of the second energy differences with the cluster size. (For interpretation of the references to colour in this figure legend, the reader is referred to the web version of this article.)

For Pd_n (n = 2–7) clusters, the variation trends of Δ_2E with the cluster size is shown in Fig. 3(b). It can be seen that the value of Δ_2E show an odd-even alternation, and two peaks appear at n = 4 and 6, indicating the special stability of Pd_4 and Pd_6 clusters. Simultaneously, it can be inferred that the Pd_8 cluster is also a magic cluster and has been confirmed in the previous work [61,69].

In addition, Pd_{13}, Pd_{19}, Pd_{23} and Pd_{38} clusters are also magic clusters of Pd_n ($n \leqslant 38$) as reported [61–65]. Their stable configurations are icosahedron, octahedron, polyicosahedron and truncated octahedron, respectively, as shown in Fig. 2. The average binding energies of Pd_{13}, Pd_{19} and Pd_{23} are 214.0, 235.0 and 239.0 kJ·mol^{-1}, respectively, agree with the reported values of 221.0, 238.0 and 244.5 kJ·mol^{-1} [60]. For Pd_{38} cluster, the average binding energy increases to 259.6 kJ·mol^{-1}, gradually approaches to the cohesive energy (375.3 kJ·mol^{-1}/Pd) [63] of Pd bulk.

The magic clusters for Pd_n ($n \leqslant 38$) are obtained according the above analysis, they are Pd_4, Pd_6, Pd_8, Pd_{13}, Pd_{19}, Pd_{23} and Pd_{38}. In the following section, the interaction between these magic clusters and the AC surface will be studied to obtain the stable Pd_n/AC sorbents.

3.3. The interaction between the magic clusters Pd_n ($n \leqslant 38$) clusters and the AC surface

3.3.1. The magic clusters Pd_n ($n \leqslant 38$) on the AC surface

The interaction between Pd_n clusters and the AC surface is discussed, and deformations of Pd_n clusters and AC are considered, similar to the case that the interaction between Au_{16} cluster and carbon defect site leads to structure distortions [73]. Thus, the interaction strength between Pd_n clusters and the AC surface is measured by the interaction energy E_{inter}, which is defined as follows:

$$E_{inter}(Pd_n/AC) = E_{ads}(Pd_n/AC) - E_{def}(AC) - E_{def}(Pd_n) \quad (7)$$

$$E_{ads}(Pd_n/AC) = E(Pd_n) + E(AC) - E(Pd_n/AC) \quad (8)$$

$$E_{def}(AC) = E'(AC) - E(AC) \quad (9)$$

$$E_{def}(Pd_n) = E'(Pd_n) - E(Pd_n) \quad (10)$$

where $E_{ads}(Pd_n/AC)$ is the adsorption energy of Pd_n cluster on the AC, and $E(Pd_n/AC)$ is the total electronic energy of AC supported Pd_n clusters in its equilibrium geometry; $E(Pd_n)$ and $E(AC)$ are total electronic energies of Pd_n cluster and AC before the interaction, while $E'(Pd_n)$ and $E'(AC)$ are values after the inteaction; $E_{def}(AC)$ and $E_{def}(Pd_n)$ are deformation energies of AC and Pd_n cluster, respectively. A positive value of interaction energy corresponds to a strong interaction between Pd_n clusters and AC. The more positive is the value, the stronger is the interaction.

Various initial configurations are considered when these magic clusters are supported on the AC surface, including interactions between the top Pd atom, the Pd-Pd bridge and the Pd-Pd-Pd surface with the C-vacancy of AC. All possible configurations and energies are shown in Fig. S2 and Table S2 in the Supporting Information. Besides, the interaction energies, deformation energies and the ratio of deformation energies to the adsorption energy for different isomeric structures are compared, and the most configurations are obtained, as shown in Fig. 4. For Pd_4 cluster, three optimized geometries Pd_4/AC(a–c) are obtained with one, two and three Pd atoms bonded to the dangling carbon at the C-vacancy site, respectively. AC has a bigger deformation than that of Pd_4 cluster during the interaction between Pd_4 cluster and AC. The deformation of AC in Pd_4/AC(a) is minimum, while in Pd_4/AC (c) is the maximum. Pd_4/AC(a) is the most stable configuration with the highest interaction energy of 428.9 kJ·mol^{-1} for Pd_4/AC, as shown in Fig. 4. However, Pd_4/AC(b) is with the highest adsorption energy of 544.6 kJ·mol^{-1}, so it was regarded as the stable structure by Jia et al. [40].

The most stable Pd_6/AC, Pd_8/AC, Pd_{13}/AC, Pd_{19}/AC, Pd_{23}/AC and Pd_{38}/AC are obtained when Pd_n clusters interact with the AC surface via the top Pd atom and the C-vacancy of AC site. It is worth mentioning that the optimized structure of Pd_{13}/AC is consistent with the previous work [74]. As listed in Table 1, AC has a bigger deformation than that of Pd_n (n = 6, 8, 13, 19, 23, 38) clusters during the interaction processes. Additionally, it can be concluded that the AC supported Pd_n (n = 4, 6, 8, 13, 19, 23, 38) clusters can stably exist for the strong interactions between Pd_n clusters and AC.

3.3.2. The influence of AC on the stability of the magic clusters Pd_n ($n \leqslant 38$)

The influence of AC on the stability of Pd_n (n = 4, 6, 8, 13, 19, 23, 38) clusters is studied. It is measured by the average binding energy difference (ΔE_b%) between bare Pd_n clusters (E_b) and the AC supported Pd_n clusters (E_b'), in which E_b can be calculated by Eq. (1); E_b' can be calculated by Eqs. (11) and (12); and ΔE_b% can be got by Eq. (13).

$$E = nE(Pd) + E(AC) - E(Pd_n/AC) \quad (11)$$

$$E_b' = (E - E_{inter})/n \quad (12)$$

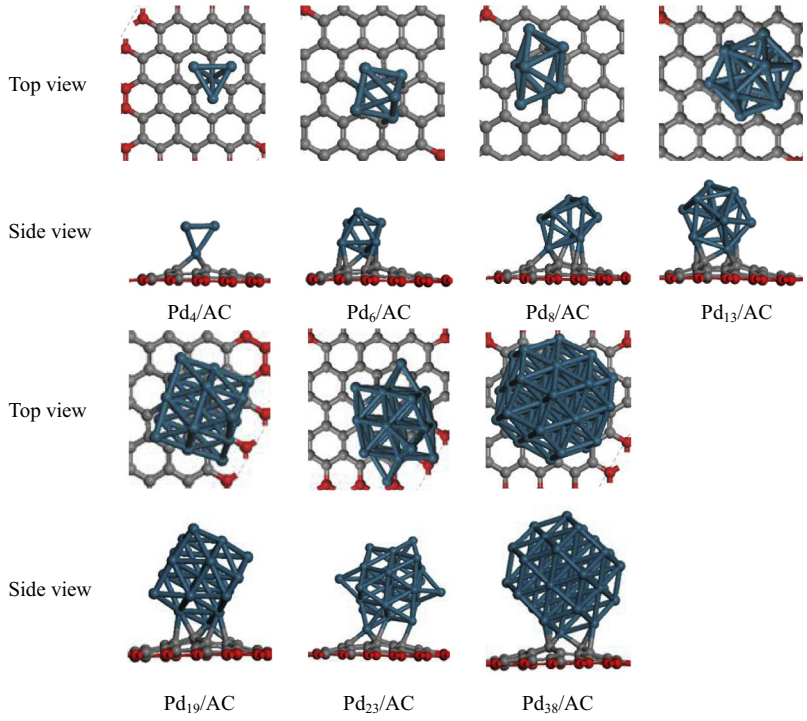

Fig. 4. The most stable configurations of magic clusters Pd_n ($n \leqslant 38$) on the AC.

Table 1
The adsorption energies E_{ads} (kJ·mol^{-1}) and interaction energies E_{inter} (kJ·mol^{-1}) involved in the most stable configurations of AC supported magic clusters Pd_n ($n \leqslant 38$), E_{def} (AC) and E_{def} (Pd_n) (kJ·mol^{-1}) represent the deformation energies of AC surface and Pd_n clusters, while ΔE_{def} (AC)% and ΔE_{def} (Pd_n)% are the ratio of deformation energy to the adsorption energy, respectively.

Structure	E_{ads}	E_{def} (AC)	ΔE_{def} (AC)%	E_{def} (Pd_n)	ΔE_{def} (Pd_n)%	E_{inter}
Pd_4	526.9	97.0	18.4	1.1	0.2	428.9
Pd_6	580.9	140.4	24.2	0.9	0.2	439.6
Pd_8	594.0	144.6	24.4	6.0	1.0	443.3
Pd_{13}	628.8	187.3	29.8	21.2	3.4	420.3
Pd_{19}	532.5	142.5	26.8	13.6	2.5	376.5
Pd_{23}	546.4	141.2	25.8	12.7	2.3	392.5
Pd_{38}	596.4	201.3	33.8	10.6	1.8	384.6

$$\Delta E_b\% = \left[\left(E'_b - E_b\right)/E_b\right] \times 100\% \quad (13)$$

The E_b and E'_b for bare and AC supported Pd_n clusters are shown in Fig. 5(a). It can be seen that the average binding energies of both bare and AC supported Pd_n clusters increase monotonously with the increase of cluster size. In addition, the existence of AC can enhance the stability of Pd_n clusters for the higher average binding energies of Pd_n clusters on AC than bare cluster [75]. However, the enhancement decreases monotonously with the increase of cluster size, nearly no effect of AC on the stability of Pd_{38} cluster, as shown in Fig. 5(b). Therefore, only AC supported Pd_n (n = 4, 6, 8, 13, 19, 23) clusters are considered to capture Hg^0.

3.4. Hg^0 adsorption on Pd_n/AC (n = 4, 6, 8, 13, 19, 23) and Pd_n cluster

For Hg^0 adsorption on the Pd_n/AC (n = 4, 6, 8, 13, 19, 23), three types of adsorption sites are taken into account, namely top (T), bridge (B) and hollow (H) sites, shown in Fig. 6. The most stable adsorption configurations are shown in Fig. 7, and the corresponding adsorption energies are shown in Fig. 8.

The stable adsorption structure for the interaction between Hg^0 and Pd_4/AC is that Hg^0 adsorbs on the top site of Pd_4/AC, with an adsorption energy of 45.3 kJ·mol^{-1}. Differently, in the most stable adsorption configurations of Hg-Pd_6/AC, Hg-Pd_8/AC and Hg-Pd_{13}/AC, Hg^0 adsorbs stably on the bridge, hollow and hollow sites with adsorption energies of 60.1, 71.6 and 84.0 kJ·mol^{-1}, respectively. The adsorption strength is in an increased order. In the most stable configurations of Hg-Pd_{19}/AC and Hg-Pd_{23}/AC, Hg^0 adsorbs on the hollow and bridge site, respectively. The adsorption energies are 62.4 and 72.4 kJ·mol^{-1}, respectively.

To sum up, with the increase of the cluster size, the adsorption site of Hg^0 on the most stable Pd_n/AC (n = 4, 6, 8, 13, 19) configurations vary from top site to bridge site then to hollow site. But abnormality is for the Pd_{23}/AC, on which bridge site is the most favorable for Hg^0 adsorption. The adsorption strength of Hg^0 on the Pd_n/AC (n = 4, 6, 8, 13, 19, 23) is in a zigzag-shape variation, as shown in Fig. 8. It can be concluded that loading the icosahedral Pd_{13} cluster on AC surface is relatively more favorable for Hg^0 adsorption, in consistent with the finding that the easiest dissociation of H_2 occurs on the Pd_{13} cluster among Pd_n (n = 4, 6, 13, 19, 55) clusters [42]. Also, it has been found that the NO adsorption energy on icosahedral-based Pd_n clusters is higher than that on the octahedral configuration [68]. Recently, the adsorption of Hg^0 on Pd/AC and Pd_{13}/AC has also been stud-

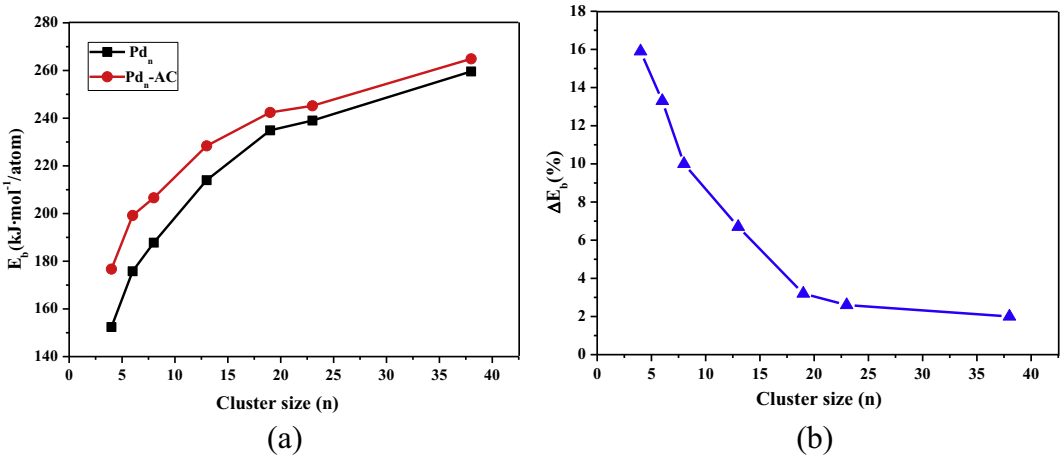

Fig. 5. (a) The average binding energy variation trends of the bare and AC supported Pd_n (n = 4, 6, 8, 13, 19, 23, 38) clusters, represented by the black and red lines, respectively; (b) the variation trend of the increased percentage ΔE_b%. (For interpretation of the references to colour in this figure legend, the reader is referred to the web version of this article.)

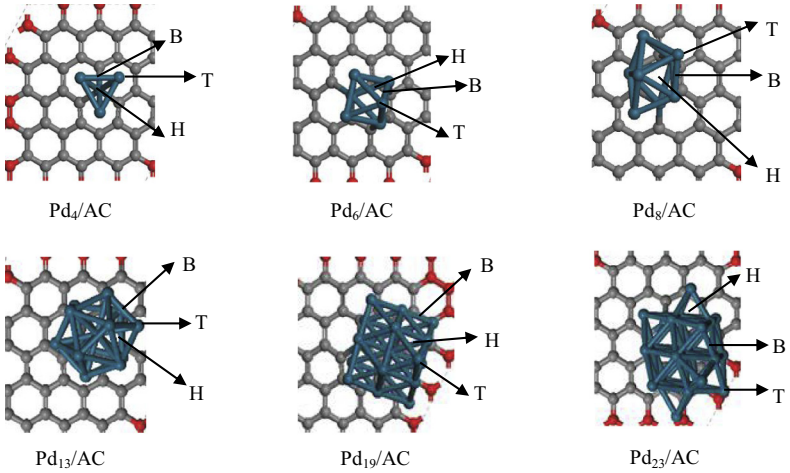

Fig. 6. The adsorption sites at the most stable Pd_n/AC (n = 4, 6, 8, 13, 19, 23) configurations.

ied, and it shows that the strength on Pd_{13}/AC is higher than that Pd/AC [76].

In addition, we remove the AC support and calculate adsorption energies of Hg^0 on bare Pd_n clusters for comparing and evaluating the effect of AC on clusters, the corresponding adsorption energies are shown in Fig. 8 (blue line). It can be seen that the energies are with little differences between Hg^0 on bare Pd clusters and Pd clusters with the same atoms supported on the AC. The largest difference occurs between Pd_{13} and Pd_{13}/AC with the energy of 11.3 kJ·mol^{-1}. This shows AC cannot enhance the adsorption of Hg^0 on Pd cluster, but can promote more electrons to transfer from support to oxygen molecule and further make the O—O bond elongation [40]. Comparing the interaction energy of Pd_n cluster on AC with the binding energy per atom of corresponding Pd_n cluster, the former is higher than that of the latter one, which shows an attractive interaction between AC and Pd clusters, and AC can disperse cluster on the surface and prevent Pd clustering to a bulk [38].

3.5. The effect of Cu modulated Pd_{13}/AC on Hg^0 adsorption

According to the above studies, it is known that the Pd_{13}/AC shows an excellent Hg^0 adsorption among Pd_n/AC (n = 4, 6, 8, 13, 19, 23). In order to increase the Hg^0 capture capacity of Pd_n/AC, meanwhile reduce the dosage of Pd, the effect of Cu modulated Pd_{13}/AC on Hg^0 adsorption is discussed in the following study.

3.5.1. The configurations and stability of Cu_nPd_{13-n} (n = 1–12) bimetallic clusters

Configurations of Cu_nPd_{13-n} (n = 1–12) bimetallic clusters with different Cu atoms substituting Pd in the most stable Pd_{13} cluster are investigated. All the possible structures and the corresponding substitution energies are shown in Fig. S3 and Table S3, respectively. The most stable configurations are shown in Fig. 9. For the $CuPd_{12}$ bimetallic cluster, the most stable configuration is that the central Pd atom of Pd_{13} cluster is substituted by one Cu atom, which is similar to configurations of $AuPd_{12}$ and $PdAu_{12}$ clusters [77]. Next, one Cu atom substituting one surface Pd atom of $CuPd_{12}$ leads to the most stable Cu_2Pd_{11} configuration. For the Cu_3Pd_{10} cluster, three isomers are obtained and their substitution energies are similar, but the structure with three Cu atoms in the center axis of Pd_{13} cluster is the most stable configuration for its high symmetry. The stable Cu-Pd clusters with 4–12 substituted Cu atoms are also obtained, as shown in Fig. 9.

The substitution energies of Cu_nPd_{13-n} (n = 1–12) bimetallic clusters are shown in Fig. 10. It can be seen that the substitution energies increase monotonously except at n = 6 with the increase

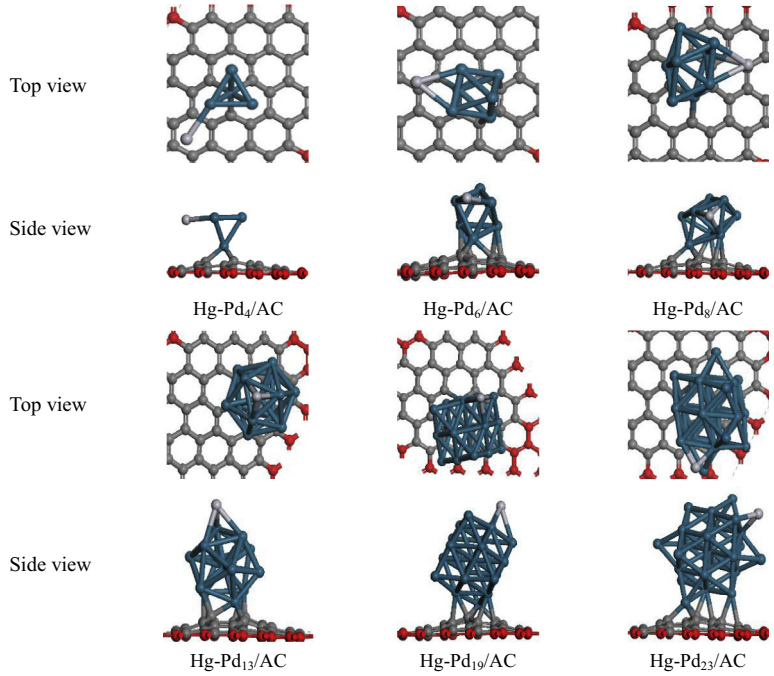

Fig. 7. The most stable adsorption configurations of Hg^0 on Pd_n/AC (n = 4, 6, 8, 13, 19, 23).

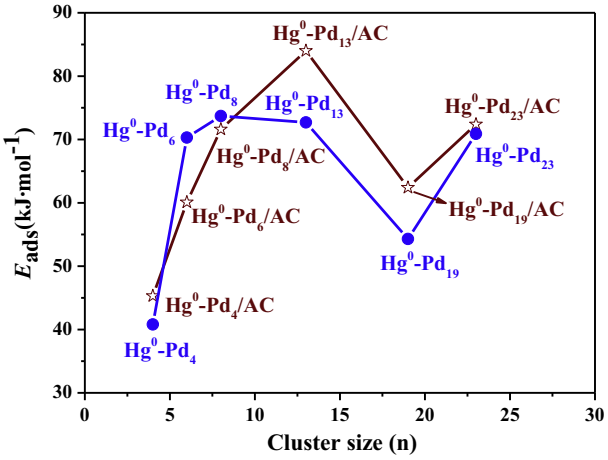

Fig. 8. The adsorption energies of Hg^0 on the Pd_n/AC and naked Pd_n (n = 4, 6, 8, 13, 19, 23) with the increase of cluster size. (For interpretation of the references to colour in this figure legend, the reader is referred to the web version of this article.)

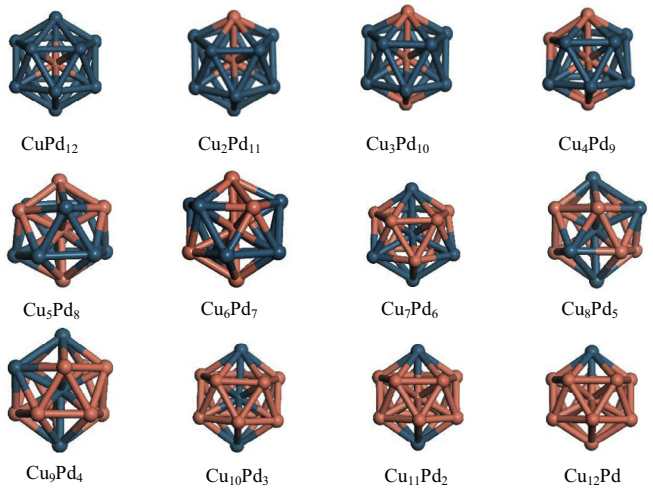

Fig. 9. The most stable configurations of Cu_nPd_{13-n} (n = 1–12) bimetallic clusters.

of substituted Cu atoms. When n = 9–12 for the substituted Cu atoms, the values of substitution energies become positive, indicating that the maximum substitution number of Cu atom for Pd_{13} cluster is eight, namely the doping ratio is 61.5%. When one, two and six Pd atoms of Pd_{13} cluster are substituted by Cu atoms, the substitution energies are relatively more negative than others, meaning $CuPd_{12}$, Cu_2Pd_{11} and Cu_6Pd_7 clusters are formed easily.

The average binding energies of Cu_nPd_{13-n} (n = 1–8) bimetallic clusters listed in Table 2 are larger than that of Pd_{13} cluster with 214.0 kJ·mol^{-1}, indicating that Cu doping can enhance the stability of Pd_{13} cluster. Combining the feasibility of Cu substitution and stability of the Cu-Pd bimetallic clusters, $CuPd_{12}$, Cu_2Pd_{11} and Cu_6Pd_7 clusters are considered to be loaded on the AC surface.

3.5.2. The interactions between Cu_nPd_{13-n}/AC (n = 1, 2, 6) and AC

The interactions between $CuPd_{12}$, Cu_2Pd_{11} and Cu_6Pd_7 bimetallic clusters and AC are discussed, which is necessary for the study

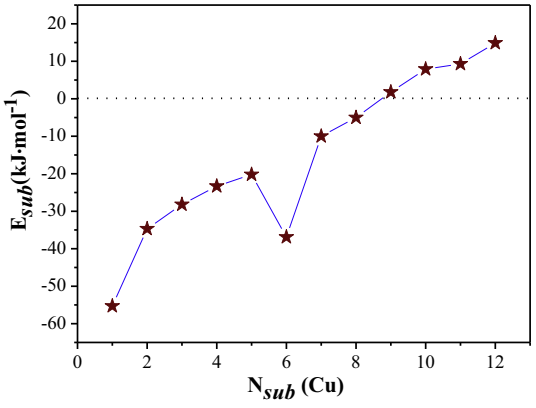

Fig. 10. The variation trends of the substitution energies of Cu_nPd_{13-n} (n = 1–12) bimetallic clusters with the substituted Cu atoms.

Table 2
The average binding energies E_b (kJ·mol^{-1}) of Cu_nPd_{13-n} (n = 1–8) bimetallic clusters.

Clusters	E_b	Clusters	E_b
$CuPd_{12}$	218.2	Cu_5Pd_8	221.7
Cu_2Pd_{11}	219.3	Cu_6Pd_7	231.0
Cu_3Pd_{10}	220.5	Cu_7Pd_6	219.3
Cu_4Pd_9	221.1	Cu_8Pd_5	217.1

of Hg^0 adsorption on the AC supported Cu-Pd bimetallic cluster. Similar to the interaction between Pd_{13} cluster and AC, two initial modes are considered, namely the top of each atom and the facet of three atoms interact with the AC, respectively. All possible configurations are shown in Figs. S4–S6, and relative energies are listed in Tables S4–S6. In addition, the interaction energies between AC and Cu-Pd bimetallic clusters are calculated to obtain the most stable AC supported Cu-Pd bimetallic clusters, which are shown in Fig. 11, and Table 3 lists the relative energies.

There are two, five and thirteen configurations for $CuPd_{12}$, Cu_2Pd_{11} and Cu_6Pd_7 bimetallic clusters interacting with AC, respectively, shown in $CuPd_{12}$/AC(a–b), Cu_2Pd_{11}/AC(a ∼ e) and Cu_6Pd_7/AC (a–m) in Figs. S4–S6. By the comparison of their interaction energies shown in Tables S4–S6, the most stable configurations of $CuPd_{12}$/AC, Cu_2Pd_{11}/AC and Cu_6Pd_7/AC are obtained. It can be seen that Pd atoms bound to the C atoms at the vacancy of AC surface, indicating that there is a strong interaction between Pd atom and sp^2 dangling bonds of these three C atoms, in consistent with other studies [34,74]. From Table 3, it can be seen that AC has a bigger deformation than that of $CuPd_{12}$, Cu_2Pd_{11} and Cu_6Pd_7 clusters. Besides, the large interaction energies indicates that $CuPd_{12}$, Cu_2Pd_{11} and Cu_6Pd_7 bimetallic clusters can stably exist on the AC surface.

3.5.3. Hg^0 adsorption on Cu_nPd_{13-n}/AC (n = 1, 2, 6)

For Hg^0 adsorption on the $CuPd_{12}$/AC, Cu_2Pd_{11}/AC and Cu_6Pd_7/AC, three types of adsorption sites including top, bridge and hollow sites are considered. The most stable adsorption configurations and corresponding adsorption energies are shown in Fig. 12 and Table 4.

Hg^0 can stably adsorb on the hollow site of $CuPd_{12}$/AC and Cu_2Pd_{11}/AC formed by three Pd atoms, and the adsorption energies are 86.8 and 106.8 kJ·mol^{-1}, respectively. Hg-Pd bond lengths are

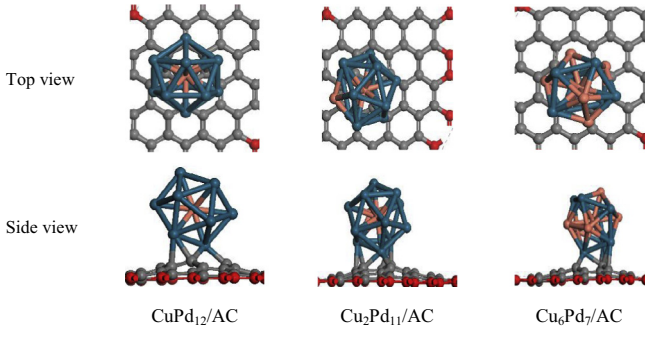

Fig. 11. The most stable configurations of $CuPd_{12}$/AC, Cu_2Pd_{11}/AC and Cu_6Pd_7/AC.

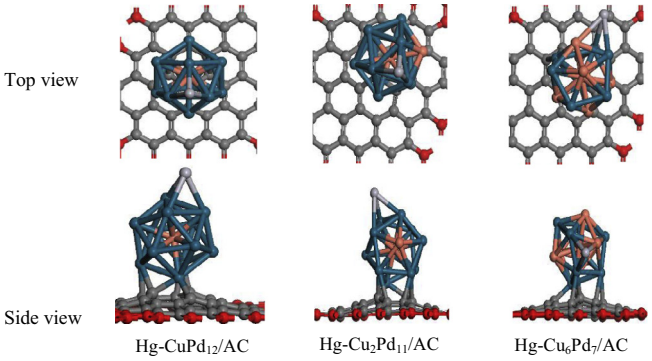

Fig. 12. The most stable configurations of Hg^0 on the Cu_2Pd_{11}/AC, Cu_6Pd_7/AC and $CuPd_{12}$/AC, including the top and side views.

Table 4
The adsorption energies E_{ads} (kJ·mol^{-1}) of Hg^0 on the most stable $CuPd_{12}$/AC, Cu_2Pd_{11}/AC and Cu_6Pd_7/AC surface.

Configuration	E_{ads}
Hg-$CuPd_{12}$/AC	86.8
Hg-Cu_2Pd_{11}/AC	106.8
Hg-Cu_6Pd_7/AC	62.9

2.815, 2.873 and 2.888 Å for Hg^0 interacting with $CuPd_{12}$/AC, and 2.843, 2.859 and 2.918 Å for Cu_2Pd_{11}/AC, respectively. On the Cu_6Pd_7/AC, Hg^0 adsorbs on the hollow site formed by one Cu atom and two Pd atoms, and the bond length of Hg-Cu is 2.991 Å, while the two Hg-Pd bonds are 2.874 and 2.896 Å, respectively. The adsorption energy is 62.9 kJ·mol^{-1}. Comparing with the adsorption energy of Hg^0 on Pd_{13}/AC, which increases by 3.3% when the doping ratio of Cu is 7.7%. It can be seen that only a slight improvement occurs for Hg^0 adsorption on $CuPd_{12}$/AC. For Cu_2Pd_{11}/AC, the adsorption energy increases greatly by 27.1% and the doping ratio of Cu is 15.4%, which is in favor of Hg^0 adsorption. However, when the number of substituted Cu atoms increases to six and the doping ratio reaches up to 46.2%, the adsorption energy decreases by 25.1%, which is unfavorable for Hg^0 adsorption. The results are well consistent with the previous result [78] that a mole fraction of Cu with 12.5–25% in Cu-Pd alloy can well promote Hg^0 adsorption, but an inhibiting effect produces when the mole fraction is more than 25%. Meanwhile, we can see that Cu_2Pd_{11}/AC is the optimal bimetal adsorbent for Hg^0.

In addition, electronic properties including Mulliken charges and partial density of states (PDOS) for Hg^0 adsorption on Cu_2Pd_{11}/AC are studied. 0.078 *e* transfers from Hg to Cu_2Pd_{11}/AC, which is higher than that on Pd_{13}/AC with 0.065 *e*, meaning that Hg^0 has a stronger interaction on Cu_2Pd_{11}/AC comparing with Pd_{13}/AC. In addition, during the interaction between Hg^0 and Cu_2Pd_{11}/AC, the PDOS for Hg-Pd bonding is analyzed, shown in Fig. 13(a–b). After the isolated Hg atom interacting with the Cu_2Pd_{11}/AC surface, all the states of Hg atom shift down, the s, *p* states broadened and

Table 3
The adsorption energies E_{ads} (kJ·mol^{-1}) and interaction energies E_{inter} (kJ·mol^{-1}) involved in the most stable AC supported $CuPd_{12}$, Cu_2Pd_{11} and Cu_6Pd_7 bimetallic clusters. E_{def} (AC) and E_{def} (cluster) (kJ·mol^{-1}) represent the deformation energies of AC surface and Cu-Pd bimetallic clusters, while ΔE_{def} (AC)% and ΔE_{def} (cluster)% are rates of the deformation energies, respectively.

Configuration	E_{ads}	E_{def} (AC)	ΔE_{def} (AC)%	E_{def} (cluster)	ΔE_{def} (cluster)%	E_{inter}
$CuPd_{12}$/AC	586.5	162.7	27.7%	12.8	2.2%	411.0
Cu_2Pd_{11}/AC	576.9	152.6	26.5%	7.1	1.2%	417.2
Cu_6Pd_7/AC	409.6	137.1	33.5%	124.9	30.5%	147.6

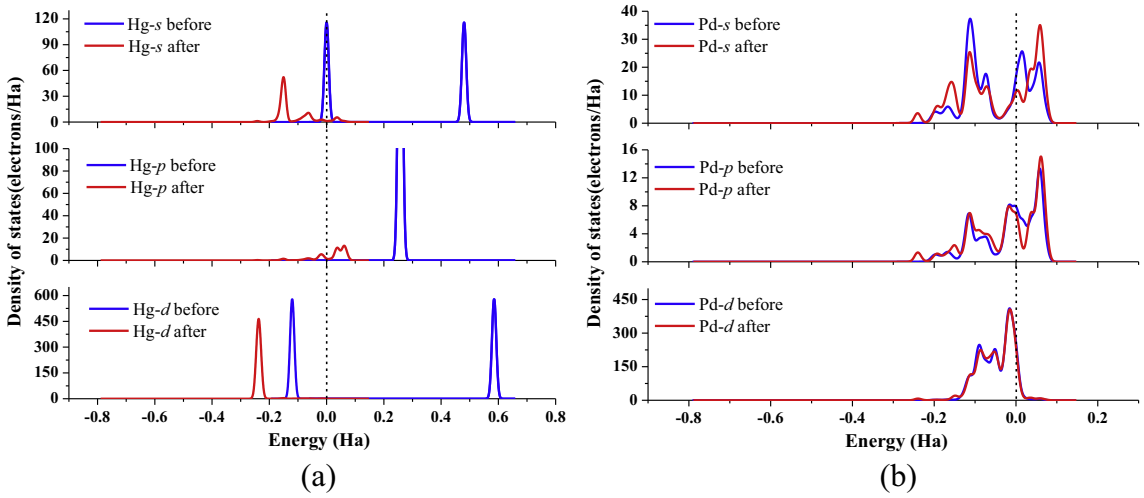

Fig. 13. The PDOS of Hg and Pd before and after interacting.

the electron density significantly reduced, implying a strong interaction between Hg^0 and the Cu_2Pd_{11}/AC surface. Differently, there's almost no change for the *d* state of Pd. It can be concluded that the *d* state of Pd nearly has no effect on the bonding, similar to the case of Hg^0 adsorption on the CuO(1 1 0) [79]. Based on the information contained after adsorption, there are overlaps between the *s* and *p* states of Hg and *p* state of Pd at approximately −0.15 and 0.07 Ha, demonstrating the bonding mechanism.

4. Conclusion

The size and Cu modulation effects on Hg^0 adsorption have been clarified by the density functional theory (DFT) method. For the size effect, activated carbon supported Pd_n ($n \leqslant 38$) clusters are used for Hg^0 adsorption. It shows that the interaction energy of Pd_n cluster on AC is higher than the binding energy per atom of corresponding Pd_n cluster, which shows AC can disperse cluster on the surface and prevent Pd clustering to a bulk. The adsorption strength of Hg^0 on Pd_n/AC (n = 4, 6, 8, 13, 19, 23) shows a zigzag-shape variation, and when loading the icosahedral Pd_{13} cluster on AC, the adsorption of Hg^0 is the strongest, with an adsorption energy of 84.0 kJ·mol^{-1}.

For the Cu modulation effect, the substitution of Pd_{13} cluster by 1–12 Cu atoms is studied, showing that Pd_{13} cluster can be substituted by eight Cu atoms at most and the Cu_nPd_{13-n} (n = 1–8) bimetallic clusters have a higher stability than that of Pd_{13} cluster. Besides, substituting one, two and six Pd atoms of Pd_{13} cluster by Cu atoms are relatively easy, and $CuPd_{12}$, Cu_2Pd_{11} and Cu_6Pd_7 bimetallic clusters can exist stably on the AC. As for the adsorption of Hg^0 on Cu-modulated Pd_{13} clusters, the doping ratios of Cu affect the adsorption greatly. Substituting the center Pd atom of Pd_{13} cluster by Cu atom has a slight improvement for Hg^0 adsorption, while increasing the number of substituted Cu atoms to two can improve the adsorption energy of Hg^0 to 106.8 kJ·mol^{-1}, in favor of Hg^0 adsorption. However, when the number of substituted Cu atoms increases to six, the adsorption energy decreases to 62.9 kJ·mol^{-1}, unfavorable for Hg^0 adsorption.

Acknowledgments

We gratefully acknowledge financial support from the National Natural Science Foundation of China (Grant Nos. 21276171, 21576178 and 21476155), Research Project Supported by Shanxi Scholarship Council of China (No. 2016-030) and the Program for the Innovative Talents of Higher Learning Institutions of Shanxi.

Appendix A. Supplementary data

Supplementary data associated with this article can be found, in the online version, at http://dx.doi.org/10.1016/j.cej.2016.09.004.

References

[1] R. Yan, D.T. Liang, L. Tsen, Y.P. Wong, Y.K. Lee, Bench-scale experimental evaluation of carbon performance on mercury vapour adsorption, Fuel 83 (2004) 2401–2409.
[2] H. Zeng, F. Jin, J. Guo, Removal of elemental mercury from coal combustion flue gas by chloride-impregnated activated carbon, Fuel 83 (2004) 143–146.
[3] J.A. Steckel, Density functional theory study of mercury adsorption on metal surfaces, Phys. Rev. B 77 (2008) 115412.
[4] L. Ling, P. Han, B. Wang, R. Zhang, Theoretical prediction of simultaneous removal efficiency of ZnO for H_2S and Hg^0 in coal gas, Chem. Eng. J. 231 (2013) 388–396.
[5] L. Ling, S. Zhao, P. Han, B. Wang, R. Zhang, M. Fan, Toward predicting the mercury removal by chlorine on the ZnO surface, Chem. Eng. J. 244 (2014) 364–371.
[6] W. Xu, H. Wang, X. Zhou, T. Zhu, CuO/TiO_2 catalysts for gas-phase Hg^0 catalytic oxidation, Chem. Eng. J. 243 (2014) 380–385.
[7] S. Niksa, N. Fujiwara, A predictive mechanism for mercury oxidation on selective catalytic reduction catalysts under coal-derived flue gas, J. Air Waste Manage. 55 (2005) 1866–1875.
[8] K.C. Galbreath, C.J. Zygarlicke, J.E. Tibbetts, R.L. Schulz, G.E. Dunham, Effects of NO_x, α-Fe_2O_3, γ-Fe_2O_3, and HCl on mercury transformations in a 7-kW coal combustion system, Fuel Process. Technol. 86 (2004) 429–448.
[9] S. Sun, D. Zhang, C. Li, Y. Wang, Q. Yang, Density functional theory study of mercury adsorption and oxidation on CuO(1 1 1) surface, Chem. Eng. J. 258 (2014) 128–135.
[10] P. Guo, X. Guo, C.G. Zheng, Computational insights into interactions between Hg species and α-Fe_2O_3(0 0 1), Fuel 90 (2011) 1840–1846.
[11] J. Liu, M. He, C. Zheng, M. Chang, Density Functional Theory study of mercury adsorption on V_2O_5(0 0 1) surface with implications for oxidation, Proc. Combust. Inst. 33 (2011) 2771–2777.
[12] L. Ling, M. Fan, B. Wang, R. Zhang, Application of computational chemistry in understanding the mechanisms of mercury removal technologies: a review, Energy Environ. Sci. 8 (2015) 3109–3133.
[13] J. Wilcox, E. Rupp, S.C. Ying, D.-H. Lim, A.S. Negreira, A. Kirchofer, F. Feng, K. Lee, Mercury adsorption and oxidation in coal combustion and gasification processes, Int. J. Coal Geol. 90–91 (2012) 4–20.
[14] D. Li, J. Han, L. Han, J. Wang, L. Chang, Pd/activated carbon sorbents for mid-temperature capture of mercury from coal-derived fuel gas, J. Environ. Sci. 26 (2014) 1497–1504.
[15] A. Jain, S.-A. Seyed-Reihani, C.C. Fischer, D.J. Couling, G. Ceder, W.H. Green, Ab initio screening of metal sorbents for elemental mercury capture in syngas streams, Chem. Eng. Sci. 65 (2010) 3025–3033.
[16] L. Geng, L. Han, W. Cen, J. Wang, L. Chang, D. Kong, G. Feng, A first-principles study of Hg adsorption on Pd(1 1 1) and Pd/γ-Al_2O_3(1 1 0) surfaces, Appl. Surf. Sci. 321 (2014) 30–37.
[17] D.-H. Lim, S. Aboud, J. Wilcox, Investigation of adsorption behavior of mercury on Au (1 1 1) from first principles, Environ. Sci. Technol. 46 (2012) 7260–7266.
[18] H.P. Zhang, X.G. Luo, H.T. Song, X.Y. Lin, X. Lu, Y. Tang, DFT study of adsorption and dissociation behavior of H_2S on Fe-doped graphene, Appl. Surf. Sci. 317 (2014) 511–516.

[19] Y. Lu, W. Chen, Sub-nanometre sized metal clusters: from synthetic challenges to the unique property discoveries, Chem. Soc. Rev. 41 (2012) 3594–3623.
[20] M. Marsault, G. Sitja, C.R. Henry, Regular arrays of Pd and PdAu clusters on ultrathin alumina films for reactivity studies, Phys. Chem. Chem. Phys. 16 (2014) 26458–26466.
[21] S. Tanabe, H. Matsumoto, Catalytic profiles of palladium clusters on zeolite in reduction of nitrogen monoxide with propane, J. Mater. Sci. Lett. 13 (1994) 1540–1542.
[22] M. Valden, J. Aaltonen, E. Kuusisto, M. Pessa, C.J. Barnes, Molecular beam studies of CO oxidation and CO-NO reactions on a supported Pd catalyst, Surf. Sci. 307 (1994) 193–198.
[23] A.S. Wörz, K. Judai, S. Abbet, U. Heiz, Cluster Size-Dependent Mechanisms of the CO + NO reaction on small $Pd_n(n \leqslant 30)$ clusters on oxide surfaces, J. Am. Chem. Soc. 125 (2003) 7964–7970.
[24] H.A. Duarte, D.R. Salahub, NO adsorption on Pd clusters. A density functional study, Top. Catal. 9 (1999) 123–133.
[25] S. Yu, X. Wang, Y. Ai, X. Tan, T. Hayat, W. Hu, X. Wang, Experimental and theoretical studies on competitive adsorption of aromatic compounds on reduced graphene oxides, J. Mater. Chem. A 4 (2016) 5654–5662.
[26] Y. Sun, S. Yang, Y. Chen, C. Ding, W. Cheng, X. Wang, Adsorption and desorption of U(VI) on functionalized graphene oxides: a combined experimental and theoretical study, Environ. Sci. Technol. 49 (2015) 4255–4262.
[27] Q.J. Lineberry, Y. Cao, Y. Lin, S. Ghose, J.W. Connell, W.-P. Pan, Mercury capture from flue gas using palladium nanoparticle-decorated substrates as injected sorbent, Energy Fuels 23 (2009) 1512–1517.
[28] C. Yue, J. Wang, L. Han, L. Chang, Y. Hu, H. Wang, Effects of pretreatment of Pd/AC sorbents on the removal of Hg^0 from coal derived fuel gas, Fuel Process. Technol. 135 (2015) 125–132.
[29] M. Sliwinska-Bartkowiak, H. Drozdowski, M. Kempinski, M. Jazdzewska, Y. Long, J.C. Palmer, K.E. Gubbins, Structural analysis of water and carbon tetrachloride adsorbed in activated carbon fibres, Phys. Chem. Chem. Phys. 14 (2012) 7145–7153.
[30] J. Greeley, I.E. Stephens, A.S. Bondarenko, T.P. Johansson, H.A. Hansen, T.F. Jaramillo, J. Rossmeisl, I. Chorkendorff, J.K. Norskov, Alloys of platinum and early transition metals as oxygen reduction electrocatalysts, Nat. Chem. 1 (2009) 552–556.
[31] M.H. Shao, T. Huang, P. Liu, J. Zhang, K. Sasaki, M.B. Vukmirovic, R.R. Adzic, Palladium monolayer and palladium alloy electrocatalysts for oxygen reduction, Langmuir 22 (2006) 10409–10415.
[32] T.H. Yu, Y. Sha, B.V. Merinov, W.A. Goddard III, Improved non-Pt alloys for the oxygen reduction reaction at fuel cell cathodes predicted from quantum mechanics, J. Phys. Chem. C 114 (2010) 11527–11533.
[33] S. Leviness, V. Nair, A.H. Weiss, Z. Schay, L. Guczi, Acetylene hydrogenation selectivity control on $PdCu/Al_2O_3$ catalysts, J. Mol. Catal. 25 (1984) 131–140.
[34] X. Liu, C. Meng, Y. Han, Defective graphene supported MPd12 (M = Fe Co, Ni, Cu, Zn, Pd) nanoparticles as potential oxygen reduction electrocatalysts: a first-principles study, J. Phys. Chem. C 117 (2013) 1350–1357.
[35] M. Xia, W. Ding, K. Xiong, L. Li, X. Qi, S. Chen, B. Hu, Z. Wei, Anchoring effect of exfoliated-montmorillonite-supported Pd catalyst for the oxygen reduction reaction, J. Phys. Chem. C 117 (2013) 10581–10588.
[36] J.P. Perdew, K. Burke, M. Ernzerhof, Generalized gradient approximation made simple, Phys. Rev. B 77 (1996) 3865–3868.
[37] J.P. Perdew, K. Burke, Y. Wang, Generalized gradient approximation for the exchange-correlation hole of a many-electron system, Phys. Rev. B 54 (1996) 16533–16539.
[38] L. Ma, J.-M. Zhang, K.-W. Xu, V. Ji, A first-principles study on gas sensing properties of graphene and Pd-doped graphene, Appl. Surf. Sci. 343 (2015) 121–127.
[39] L. Jeloaica, V. Sidis, DFT investigation of the adsorption of atomic hydrogen on a cluster-model graphite surface, Chem. Phys. Lett. 300 (1999) 157–162.
[40] T.-T. Jia, C.-H. Lu, K.-N. Ding, Y.-F. Zhang, W.-K. Chen, Oxidation of Pd_n (n = 1–5) clusters on single vacancy graphene: a first-principles study, Comput. Theor. Chem. 1020 (2013) 91–99.
[41] C. Luo, C. Zhou, J. Wu, T.J. Dhilip Kumar, N. Balakrishnan, R.C. Forrey, H. Cheng, First principles study of small palladium cluster growth and isomerization, Int. J. Quantum Chem. 107 (2007) 1632–1641.
[42] X. Liu, D. Tian, C. Meng, DFT study on the adsorption and dissociation of H_2 on Pd_n (n = 4, 6, 13, 19, 55) clusters, J. Mol. Struct. 1080 (2015) 105–110.
[43] B. Delley, From molecules to solids with the $DMol^3$ approach, J. Chem. Phys. 113 (2000) 7756–7764.
[44] B. Delley, An all-electron numerical method for solving the local density functional for polyatomic molecules, J. Chem. Phys. 92 (1990) 508–517.
[45] L. Wang, Q. Luo, W. Zhang, J. Yang, Transition metal atom embedded graphene for capturing CO: a first-principles study, Int. J. Hydrogen Energy 39 (2014) 20190–20196.
[46] P.J. Hay, W.R. Wadt, Ab initio effective core potentials for molecular calculations. Potentials for K to Au including the outermost core orbitals, J. Chem. Phys. 82 (1985) 299–310.
[47] X.-Q. Liu, Y. Xue, Z.-Y. Tian, J.-J. Mo, N.-X. Qiu, W. Chu, H.-P. Xie, Adsorption of CH_4 on nitrogen- and boron-containing carbon models of coal predicted by density-functional theory, Appl. Surf. Sci. 285 (2013) 190–197.
[48] Y.-H. Lu, M. Zhou, C. Zhang, Y.-P. Feng, Metal-embedded graphene: a possible catalyst with high activity, J. Phys. Chem. C 113 (2009) 20156–20160.
[49] D.-H. Lim, J. Wilcox, DFT-based study on oxygen adsorption on defective graphene-supported Pt nanoparticles, J. Phys. Chem. C 115 (2011) 22742–22747.
[50] L. Fan, L. Ling, B. Wang, R. Zhang, The adsorption of mercury species and catalytic oxidation of Hg^0 on the metal-loaded activated carbon, Appl. Catal. A 520 (2016) 13–23.
[51] Y. Liu, J. Wilcox, CO_2 adsorption on carbon models of organic constituents of gas shale and coal, Environ. Sci. Technol. 45 (2011) 809–814.
[52] T. Haugan, P.N. Barnes, R. Wheeler, F. Meisenkothen, M. Sumption, Addition of nanoparticle dispersions to enhance flux pinning of the $YBa_2Cu_3O_{7-x}$ superconductor, Nature 430 (2004) 867–870.
[53] P. Cabrera-Sanfelix, Adsorption and reactivity of CO_2 on defective graphene sheets, J. Phys. Chem. A 113 (2009) 493–498.
[54] Q. Chen, C. Tang, G. Zheng, First-principles study of TiO_2 anatase (1 0 1) surfaces doped with N, Physica B 404 (2009) 1074–1078.
[55] G. Wang, R. Zhang, B. Wang, Insight into the preference mechanism for C–C chain formation of C_2 oxygenates and the effect of promoters in syngas conversion over Cu-based catalysts, Appl. Catal. A 466 (2013) 77–89.
[56] Y. Liu, Elemental Mercury Removal from Flue Gas by Metal/Metal Oxide Decorated Graphene Oxide Composites, University of Alberta, 2014.
[57] E.J. Granite, C.R. Myers, W.P. King, D.C. Stanko, H.W. Pennline, Sorbents for mercury capture from fuel gas with application to gasification systems, Ind. Eng. Chem. Res. 45 (2006) 4844–4848.
[58] I. Efremenko, E.D. German, M. Sheintuch, Density functional study of the interactions between dihydrogen and Pd_n (n = 1–4) clusters, J. Phys. Chem. A 104 (2000) 8089–8096.
[59] Y. Okamoto, Density-functional calculations of atomic and molecular adsorptions on 55-atom metal clusters: comparison with (1 1 1) surfaces, Chem. Phys. Lett. 405 (2005) 79–83.
[60] V. Kumar, Y. Kawazoe, Icosahedral growth, magnetic behavior, and adsorbate-induced metal-nonmetal transition in palladium clusters, Phys. Rev. B 66 (2002).
[61] B. Kalita, R.C. Deka, Density functional studies on structure and reactivity of Pd_n clusters for n = 1–13, Bull. Catal. Soc. India 5 (2006) 110–120.
[62] F. Aguilera-Granja, A. García-Fuente, A. Vega, Comparative *ab initio* study of the structural, electronic, and magnetic trends of isoelectronic late 3d and 4d transition metal clusters, Phys. Rev. B 78 (2008).
[63] M. Karabacak, S. Özçelik, Z.B. Güvenç, Structures and energetics of Pd_n (n = 2–20) clusters using an embedded-atom model potential, Surf. Sci. 507–510 (2002) 636–642.
[64] G. Wang, Genetic algorithm in atomic cluster research, Prog. Phys. 20 (2000) 251–275.
[65] S. Krüger, S. Vent, F. Nörtemann, M. Staufer, N. Rösch, The average bond length in Pd clusters Pd[sub n], n = 4-309: a density-functional case study on the scaling of cluster properties, J. Chem. Phys. 115 (2001) 2082.
[66] P. Nava, M. Sierka, R. Ahlrichs, Density functional study of palladium clusters, Phys. Chem. Chem. Phys. 5 (2003) 3372–3381.
[67] R. Robles, S.N. Khanna, Oxidation of Pd_n(n = 1–7, 10) clusters supported on alumina/NiAl(1 1 0), Phys. Rev. B 82 (2010) 2283–2288.
[68] X. Liu, D. Tian, S. Ren, C. Meng, Structure sensitivity of NO adsorption–dissociation on Pd_n(n = 8, 13, 19, 25) clusters, J. Phys. Chem. C 119 (2015) 12941–12948.
[69] J.N. Li, Theoretical Study on the Adsorption and Catalysis of the Pdn Clusters and Their Supported Catalytic Materials, Beijing University of Technology, 2012.
[70] B.C. Guo, S. Wei, J. Purnell, S. Buzza, J.A.W. Castleman, Metallo-carbohedrenes $[M_8C_{12}^+(M = V, Zr, Hf, and Ti)]$: a class of stable molecular cluster ions, Science 256 (1992) 515–516.
[71] M. Boyukata, J.C. Belchior, Molecular dynamics study of palladium clusters size dependent analysis of structural stabilities and energetics of $Pd_n(n \leqslant 40)$ via a Lennard-Jones type potential, Croat. Chem. Acta 81 (2008) 289–298.
[72] S.K. Nayak, P. Jena, V.S. Stepanyuk, W. Hergert, K. Wildberger, Magic numbers in supported metal clusters, Phys. Rev. B 56 (1997) 6952–6957.
[73] A.J. Logsdail, J. Akola, Interaction of Au_{16} nanocluster with defects in supporting graphite: a density-functional study, J. Phys. Chem. C 115 (2011) 15240–15250.
[74] X. Liu, L. Li, C. Meng, Y. Han, Palladium nanoparticles/defective graphene composites as oxygen reduction electrocatalysts: a first-principles study, J. Phys. Chem. C 116 (2012) 2710–2719.
[75] I. Cabria, M.J. López, J.A. Alonso, Theoretical study of the transition from planar to three-dimensional structures of palladium clusters supported on graphene, Phys. Rev. B 81 (2010).
[76] J. Meeprasert, A. Junkaew, C. Rungnim, M. Kunaseth, N. Kungwan, V. Promarak, S. Namuangruk, Capability of defective graphene-supported Pd_{13} and Ag_{13} particles for mercury adsorption, Appl. Surf. Sci. 364 (2016) 166–175.
[77] W. Zhang, D. Cheng, J. Zhu, Theoretical study of CO catalytic oxidation on free and defective graphene-supported Au–Pd bimetallic clusters, RSC Adv. 4 (2014) 42554–42561.
[78] S. Aboud, E. Sasmaz, J. Wilcox, Mercury adsorption on PdAu, PdAg and PdCu alloys, Main Group Chem. 7 (2008) 205–215.
[79] W. Xiang, J. Liu, M. Chang, C. Zheng, The adsorption mechanism of elemental mercury on CuO (1 1 0) surface, Chem. Eng. J. 200–202 (2012) 91–96.